Nuclear level density and γ-ray strength function of ^{43}Sc

A. Bürger,[1] A. C. Larsen,[1,*] S. Hilaire,[2] M. Guttormsen,[1] S. Harissopulos,[3] M. Kmiecik,[4] T. Konstantinopoulos,[3]
M. Krtička,[5] A. Lagoyannis,[3] T. Lönnroth,[6] K. Mazurek,[4] M. Norrby,[6] H. T. Nyhus,[1] G. Perdikakis,[3,†]
S. Siem,[1] A. Spyrou,[3,†] and N. U. H. Syed[1]

[1]*University of Oslo, Department of Physics, N-0316 Oslo, Norway*
[2]*CEA, DAM, DIF, F-91297 Arpajon, France*
[3]*Institute of Nuclear Physics, NCSR "Demokritos", 153.10 Aghia Paraskevi, Athens, Greece*
[4]*Institute of Nuclear Physics PAN, Kraków, Poland*
[5]*Institute of Nuclear and Particle Physics, Charles University, Prague, Czech Republic*
[6]*Physics, Department of Natural Sciences, Åbo Akademi University, FIN-20500 Åbo, Finland*

The nuclear level density and the γ-ray strength function have been determined for ^{43}Sc in the energy range up to 2 MeV below the neutron separation energy using the Oslo method with the 46Ti$(p, \alpha)^{43}$Sc reaction. A comparison to ^{45}Sc shows that the level density of ^{43}Sc is smaller by an approximately constant factor of two. This behavior is well reproduced in a microscopic, combinatorial model calculation. The γ-ray strength function increases at low γ-ray energies, a feature which has been observed in several nuclei but which still awaits theoretical explanation.

PACS number(s): 21.10.Ma, 21.10.Pc, 25.40.Hs, 27.40.+z

I. INTRODUCTION

Network calculations aiming to reproduce isotopic abundances observed in stars or predictions of isotope productions in nuclear power plants require good knowledge of nuclear level densities and γ-ray transition rates for many nuclei and over a large range of excitation energies to calculate the relevant cross sections. Up to a certain excitation energy, it is feasible to perform spectroscopic measurements on all individual nuclear excited states and to determine at least some of their properties. But at higher excitation energies, the spacing between nuclear levels may become very small, which does not allow us to resolve all individual levels. A continuing effort has long been devoted both in experiment and theory to the study of level densities and γ-ray strength functions also in this region of the quasicontinuum. Despite these efforts, the amount of available experimental data is relatively small. Therefore, network calculations often have to rely on models to compensate for the lack of measured values, and models are difficult to validate without experimental data to compare with.

The nuclear physics group at the University of Oslo has performed many experiments using the Oslo method to determine nuclear level densities and γ-ray strength functions of many isotopes throughout the nuclear chart [1–6]. In the present work, the Oslo method is used on a nucleus produced in a (p, α) reaction to determine the level density and the γ-ray strength function of ^{43}Sc. Previously published data for ^{45}Sc [2], produced in the $(^3$He,^{3}He$')$ reaction, allow the comparison of two relatively light isotopes with $\Delta A = 2$.

In the next section, the experimental setup and the analysis procedure are described, followed by a discussion of the experimental results in Secs. III and IV. In Sec. V, we conclude with a summary.

II. EXPERIMENT AND DATA ANALYSIS

The experiment was performed at the cyclotron laboratory of the University of Oslo. A proton beam with an energy of 32 MeV impinged on a Ti target of 3 mg/cm^2 thickness with an enrichment of 86% 46Ti. The main impurities were ^{48}Ti (10.6%), ^{47}Ti (1.6%), ^{50}Ti (1.0%), and ^{49}Ti (0.8%). Eight silicon $\Delta E - E$ particle telescopes with a total geometric efficiency of about 1.3% were placed in the forward direction 5 cm behind the target at an angle of 45° with respect to the beam axis. The target was surrounded by the γ-ray detector array CACTUS, consisting of 28 collimated NaI(Tl) scintillator crystals covering about 15% of 4π.

Using the specific energy losses in the thin (140 μm) ΔE and the thick (1500 μm) E particle detectors, α ejectiles were identified to select the 46Ti$(p, \alpha)^{43}$Sc reaction channel. From the known Q values, the reaction kinematics and the energy losses in the materials passed by the α particles, the initial excitation energies E_i of the ^{43}Sc nuclei could be reconstructed with an accuracy of about 700 keV full width at half maximum (FWHM).

The difference in total energy deposit in the Si detectors between ^{43}Sc (produced from the main target component, 46Ti) and ^{45}Sc (produced from the main impurity, ^{48}Ti) in the respective (p, α) reactions is only about 0.5 MeV for the ground states. With the present experimental setup, it is not possible to separate the reactions on the two target components and a certain level of background from ^{45}Sc cannot be removed from the spectra for ^{43}Sc.

From the amount of impurities in the target, one would expect that the contribution from these impurities should not exceed $\approx$14%. This assumption is supported by (p, t) data
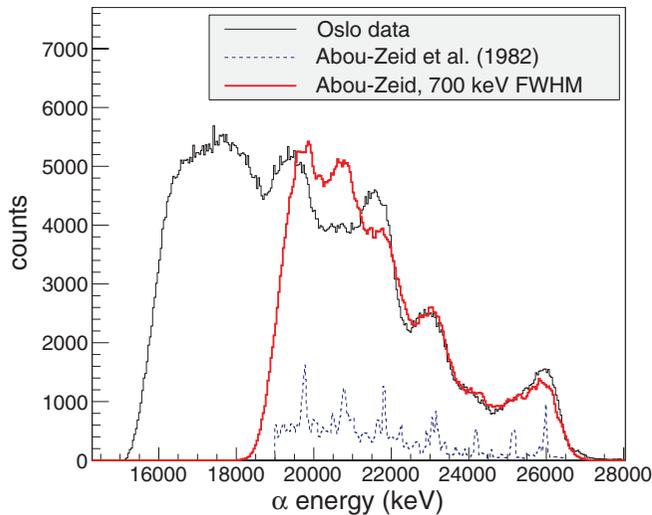

FIG. 1. (Color online) Alpha spectra from the $46\text{Ti}(p,\alpha)^{43}\text{Sc}$ reaction: Oslo data from one particle telescope (black solid line), data from Abou-Zeid *et al.* scaled by a factor of 10 (blue dashed line, from Ref. [8]), and the Abou-Zeid data folded with a Gaussian of 700 keV FWHM and scaled by a factor of 40 (red line).

from the same experiment (see Fig. 2 in Ref. [7]). Here, it is clear that the main impurity is stemming from $(p,t)46\text{Ti}$, which is of the order of 10%. In addition, from calculations of differential cross sections at 45° for the $(p,\alpha)^{43,45}\text{Sc}$ reactions and from the cross-section data of Ref. [8], we find no significant difference in either the absolute value nor the shape of the estimated α spectra. Therefore, it seems reasonable to believe that the background from ^{45}Sc in the present data is of the same order as the amount of ^{48}Ti in the target.

A comparison with the ^{43}Sc α-particle spectrum from Ref. [8], folded with the present detector resolution, shows very good agreement for α energies above ≈ 22 MeV (see Fig. 1). This further indicates that the contribution from ^{45}Sc is rather small.

We observe deviations between our data and the Abou-Zeid data for $E_\alpha < 21$ MeV. In particular, this is so for the peaks centered at ≈ 21.6 MeV and ≈ 19.5 MeV in our data, and the peak at ≈ 20.7 MeV in the Abou-Zeid data. The former ones are coming by the $^{16}\text{O}(p,\alpha)^{13}\text{N}$ reaction, as the Ti target had a layer of TiO_2 on the surface. However, there is no obvious reason for the difference of the latter peak. Possibly, the different beam energy and scattering angle (our data cover angles between $\approx 43°$–$47°$) could account for the observed deviation.

As a consequence of the ^{45}Sc contribution, some smoothing effects on the extracted quantities are expected.

The excited ^{43}Sc nuclei will emit cascades of γ rays to decay to their ground states. The spectra of these γ-ray energies E_γ were measured in coincidence with the α particles, and a matrix E_i vs E_γ was constructed after correcting for the NaI response function, as described in Ref. [9]. This matrix of unfolded γ-ray spectra was normalized such that, for each initial excitation energy E_i, the integral over all γ-ray energies measured in coincidence with this excitation energy equaled the average

γ-ray multiplicity observed in this excitation energy bin. The average multiplicity was determined as $\langle M \rangle = E_i/\langle E_\gamma \rangle$ with the average γ-ray energy $\langle E_\gamma \rangle$ for the excitation energy bin E_i [10]. The first-generation method [11] was then applied on this matrix to extract a matrix P containing the spectrum of primary γ-ray energies for each initial excitation energy bin E_i. A fundamental assumption for the first-generation method is that the γ-ray spectrum emitted from each excitation energy bin is independent of how the states in this bin were populated—by γ decay from higher excited states or by population in the (p,α) reaction.

From the matrix P, both the shape of the level density $\rho(E_f)$ and the shape of the γ-ray strength function $f(E_\gamma)$ can be extracted as described in Ref. [9]. As explained there, this extraction can only be performed if the γ-ray strength function only depends on the γ-ray energy, but not on the excitation energy (the generalized Brink-Axel hypothesis [12,13]), and the transition probability from an initial state i to a final state f (with excitation energies E_i and E_f, respectively) can be factorized into the level density at the final state, $\rho(E_f)$, and the γ transmission coefficient, $\mathcal{T}(E_i - E_f)$. Furthermore, it is assumed in the following that dipole radiation is predominant and that one can write $\mathcal{T}(E_\gamma) = 2\pi f(E_\gamma)E_\gamma^3$. The results obtained at this point are only the functional forms of ρ and f in the sense that the matrix P can be equally fit to other pairs of ρ' and f' obtained by the transformations:

$$\rho'(E_f) = A \exp(\alpha E_f)\rho(E_f), \qquad (1)$$

$$f'(E_\gamma) = B \exp(\alpha E_\gamma)f(E_\gamma), \qquad (2)$$

for any positive values of A, B, and any value of α [9].

To determine appropriate values for these coefficients, the level density and the γ-ray strength function must be normalized using data from other sources. The parameters A and α were determined using two level-density values: one is the counted level density from discrete-line spectroscopy at low excitation energy, where it has been assumed that all levels have been observed (green region in Fig. 2). The second is the level density derived from resonance spacings at average energy E_n, slightly above a particle separation energy. This value is extrapolated to lower excitation energies using a scaled back-shifted Fermi gas (BSFG) model [14] to bridge the gap between the maximum energy for which $\rho(E_f)$ can be determined in the experiment and E_n (red line and region in Fig. 2). While no neutron resonance data are available for ^{43}Sc, some information on proton resonances is tabulated in Ref. [15]. To perform the normalization, it has been assumed that the tentative spin assignments in Ref. [15] are correct and that the distribution of unknown spin-parity values equals the distribution of known spin-parity values. The normalization point for the level density has then been obtained by counting the levels in the excitation energy region around $E_n = 7$ MeV. The BSFG parameters for the extrapolation are the same as used for ^{45}Sc in [2]: the level-density parameter was $a = 4.94$ MeV^{-1}, the back-shift parameter $E_1 = -2.55$ MeV. In addition, the curve was scaled with a factor $\eta = 0.585$ to match the level-density normalization point for ^{43}Sc as obtained from the proton resonance data. This particular BSFG
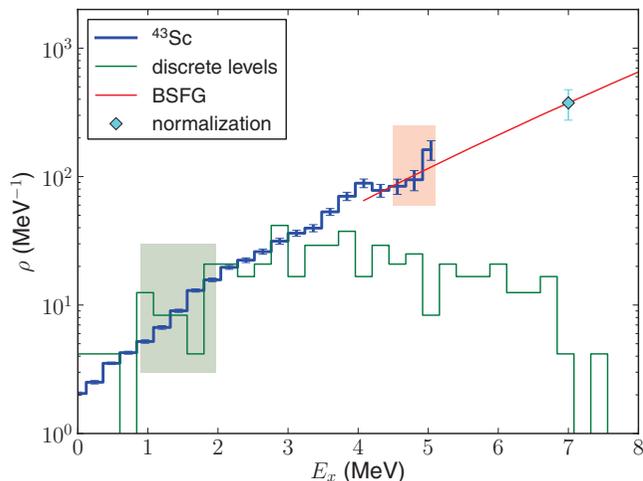
FIG. 2. (Color online) Experimental level density for ^{43}Sc. The experimental curve (blue steps) is normalized to discrete levels (green steps, fit in green region) and to proton resonance spacings (cyan diamond) extrapolated using a BSFG model (red line, fit in the red region).

FIG. 3. (Color online) Level-density comparison. The experimental level density for ^{43}Sc (blue steps) is compared to the experimental level density of ^{45}Sc (red steps) [2] and to combinatorial model calculations for these two nuclei (blue and red lines for ^{43}Sc and ^{45}Sc, respectively), see text. In addition, BSFG calculations are included for ^{43}Sc and ^{45}Sc (blue and red dashed lines, respectively).

parametrization was chosen to allow a comparison with the data for ^{45}Sc from Ref. [2].

A third normalization point is necessary to fix the parameter B for the γ-ray strength function scale. If available, data on the average total radiative width could be used for this purpose [16,17]. Such data are, however, not available for ^{43}Sc. Therefore, estimated values of the γ-ray strength function for ^{46}Sc have been used in exactly the same way as for ^{45}Sc in Ref. [2]: the normalization value is the sum of the $E1$ and $M1$ strength function values for ^{46}Sc from Ref. [18]. The use of the ^{46}Sc value is justified if it is assumed that the γ-ray strength functions for ^{43}Sc and ^{46}Sc (and ^{45}Sc) are not very different in scale.

III. NUCLEAR LEVEL DENSITY

Figure 2 shows the level-density curve obtained for ^{43}Sc after the normalization as described in the previous section. The level-density normalization point at $E_n = 7$ MeV is $\rho(E_n) = 375$ MeV^{-1} with an estimated uncertainty of $\Delta\rho(E_n) = 100$ MeV^{-1}. The uncertainties for the experimental data points in this figure are estimated mainly based on the number of counts in the E_i vs E_γ matrices (see Ref. [9]). They do, in particular, not include the uncertainty from the normalization. In Fig. 3, the experimental level density is compared to the previously published level-density curve for ^{45}Sc [2]. It appears that, on a logarithmic scale, the two level-density curves are more or less parallel to each other: the level density for ^{45}Sc is larger by a factor of about 2 for a large excitation-energy range. A similar behavior has been found in heavier nuclei: near closed shells, the level density of nuclei of the same element with masses A and $(A+2)$ differs significantly [1,5,19]. For midshell nuclei, on the other hand, the level density of $\Delta A = 2$ neighbors of the same element is very similar or almost identical in scale [20,21].
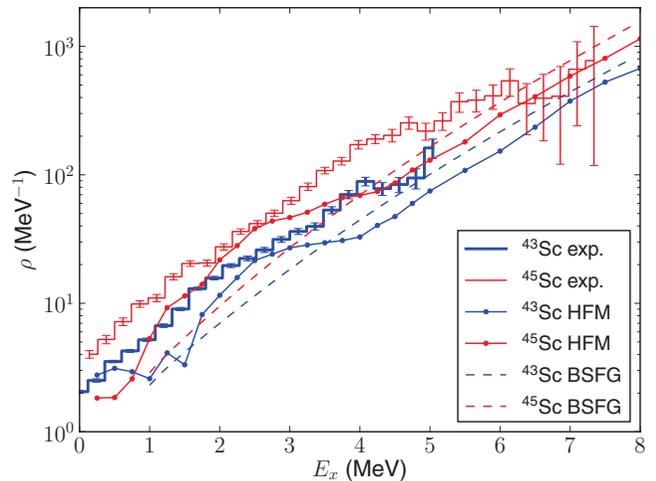
It is not obvious from where this increase by a factor 2 between $A = 43$ and $A = 45$ originates. In case of spherical nuclei with pronounced $N = 20$ and $N = 28$ shell gaps, only a few active particles in the $f_{7/2}$ orbitals would be responsible for the number of levels; namely, 1 π and 2 ν for ^{43}Sc, and 1 π and 4 ν for ^{45}Sc. In this picture, one could expect many more configurations at one and the same excitation energy for ^{45}Sc compared to ^{43}Sc. However, both isotopes have an $I^\pi = 3/2^+$ state just above the $7/2^-$ ground state, indicating that the $d_{3/2}$ hole orbital is close to the $f_{7/2}$, which can be explained by a quadrupole deformation of $\epsilon_2 \approx 0.23$ as shown in the Nilsson single particle scheme of Ref. [2]. These calculations show a rather uniform distribution of Ω^π Nilsson orbitals, and one could expect very similar level densities for ^{45}Sc and ^{43}Sc. On the other hand, it is well established that ^{45}Sc exhibits coexistence of prolate and weakly oblate (nearly spherical) rotational bands [22]. Since the level density includes all types of configurations with various spins and parities, one has to expect contributions from both shapes, where the near-spherical shape might drive toward a large level-density ratio and the deformed shape toward a small level-density ratio between ^{43}Sc and ^{45}Sc. The situation is complex and it is difficult to present simple arguments to explain the experimentally observed level-density ratio of $\approx$2.

Figure 3 includes calculations of level densities for ^{43}Sc and ^{45}Sc using the phenomenological BSFG model. For these curves, the global parametrization from [23] was used (which is different from the parameters used for the normalization in Sec. II and Fig. 2). This parametrization includes shell effects via nuclear masses, which enter the calculation of the level-density parameter a. The resulting ratio of level densities is 1.5 at $E_x = 3$ MeV, slightly smaller than the ratio of 2 seen in experiment. Generally, the two BSFG calculations tend to underestimate the level density below $E_x = 6$ MeV.

TABLE I. Microscopical model normalization parameters. The values for the level-density normalization energy E_n and density $\rho(E_n)$ for ^{45}Sc are from Ref. [2], and the values for ρ_{HFM} were interpolated from Ref. [25].

Nucleus	E_n (MeV)	$\rho(E_n)$ (MeV^{-1})	$\rho_{HFM}(E_n)$ (MeV^{-1})	c
^{43}Sc	7.0	375	1022	-0.379
^{45}Sc	9.904	3701	11470	-0.359

Figure 3 also includes theoretical level-density curves derived from calculations using the combinatorial plus Hartree-Fock-Bogoliubov model (HFM) described in Ref. [24]. These theoretical level densities were retrieved from Ref. [25]. As explained in Ref. [24], a meaningful comparison of the theoretical predictions ρ_{HFM} with the experimental data ρ_{exp} requires a normalization of ρ_{HFM} to the level-density value used to normalize the experimental level densities at a given energy E_n. Following the normalization recipe of Ref. [23], we thus determine for both of ^{43}Sc and ^{45}Sc a normalization parameter c such that

$$\rho_{HFM}(E_n)\exp(c\sqrt{E_n}) = \rho_{exp}(E_n), \qquad (3)$$

and then plot in Fig. 3 the normalized values; that is,

$$\rho_{HFM}(E_x)\exp(c\sqrt{E_x}), \qquad (4)$$

as a function of E_x.

In Fig. 3, we chose zero pairing shift and obtained values for c from Eq. (3) as listed in Table I. The normalized HFM curves nearly reproduce the parallel trend of the level-density curves and the ratio between them with a significant increase of the ^{45}Sc level densities with respect to that of ^{43}Sc, but they underestimate the level densities for both nuclei. The main qualitative differences between the HFM calculation and experimental data are at excitation energies below 1.5 MeV, where the calculation neither reproduces the level densities as obtained from discrete level counting nor their ratio, and in the excitation energy range between around 1.5 and 4 MeV where the model predicts a local increase in the level density for both nuclei which is not seen in experiment.

At excitation energies below 2 MeV, the HFM curves show more structure than the experimental curves. One possible explanation is the experimental energy resolution. Another possibility to explain this mismatch is the too-approximate treatment of the coupling between particle-hole and vibrational excitations implemented in the combinatorial HFM model. To check this hypothesis, we tested a simplistic model to mimic a more realistic particle-vibration coupling resulting in a spreading of the coupled states by an arbitrarily chosen energy of the order of a few hundred keV. The HFM curves obtained using such a simplistic treatment show, as expected, less structure and better agreement with the shape of the experimental data. The tested modifications are, however, completely arbitrary and have to be investigated and refined in future work before including them in the general HFM calculations.
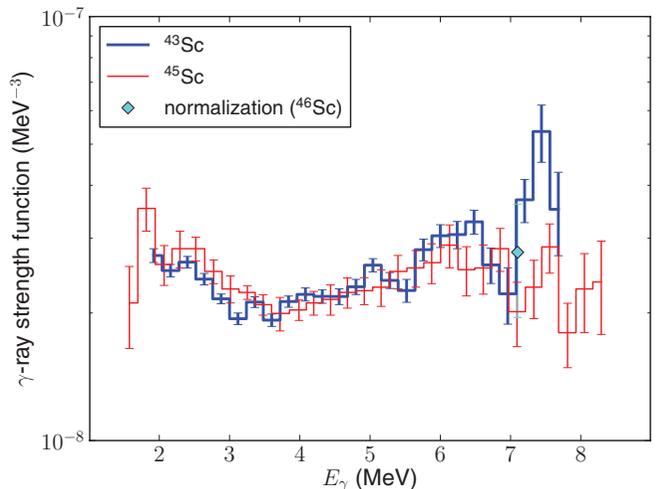

FIG. 4. (Color online) γ-ray strength function for ^{43}Sc. The experimental curve (blue steps) is shown together with the γ-ray strength function for ^{45}Sc (red steps). The normalization data point from ^{46}Sc is also shown (cyan diamond).

IV. GAMMA-RAY STRENGTH FUNCTION

Figure 4 shows the experimental curves of the γ-ray strength function for ^{43}Sc, together with the experimental data for ^{45}Sc [2]. As for the level density, the uncertainties for the experimental data points are estimated mainly based on the number of counts in the E_i vs E_γ matrices. The similarity of the shapes of the measured γ-ray strength functions of the $\Delta A = 2$ neighbors is astonishing. A common feature of the curves is that they both show a minimum at around 3.5 MeV and an increase of the γ-ray strength function for lower γ-ray energies. Similar behavior has been observed in other nuclei and using different experimental approaches [17,26–28].

A possible explanation for the case of light nuclei is the typically low level density at low excitation energy, in particular the scarcity of higher-spin states, and the dominance of $E1$ radiation. For a higher-spin state—which can be populated in the particle-induced reaction—the deexcitation then needs multiple, smaller-energy steps to reach one of the available low-spin states at low excitation energy [29].

Phenomenological models describing such γ-ray strength functions shows that the increased γ-ray strength for low E_γ may have important effects on radiative neutron capture cross sections and thus on r-process nucleosynthesis calculations [30].

V. SUMMARY

The nuclear level density and the γ-ray strength function of ^{43}Sc have been determined experimentally using the Oslo method. There is an almost constant factor between the level densities of ^{43}Sc and ^{45}Sc, a behavior similar to what has been observed in heavier nuclei in the vicinity of shell closures. The parallel evolution of the level densities of the two $\Delta A = 2$ isotope neighbors can be nearly reproduced

within a combinatorial model for a large excitation energy range. The γ-ray strength function for ^{43}Sc is surprisingly similar to the one of ^{45}Sc, and it shows an increase at low γ-ray energy which cannot be explained theoretically as of yet.

[1] R. Chankova *et al.*, Phys. Rev. C **73**, 034311 (2006); see also M. Guttormsen *et al.*, arXiv:0801.4667.

[2] A. C. Larsen *et al.*, Phys. Rev. C **76**, 044303 (2007).

[3] E. Algin *et al.*, Phys. Rev. C **78**, 054321 (2008).

[4] U. Agvaanluvsan *et al.*, Phys. Rev. C **79**, 014320 (2009).

[5] N. U. H. Syed *et al.*, Phys. Rev. C **79**, 024316 (2009).

[6] H. T. Nyhus *et al.*, Phys. Rev. C **81**, 024325 (2010).

[7] A. C. Larsen *et al.*, Phys. Rev. C **85**, 014320 (2012).

[8] O. A. Abou-Zeid *et al.*, Nucl. Phys. A **382**, 185 (1982).

[9] A. Schiller *et al.*, Nucl. Instr. Meth. A **447**, 498 (2000).

[10] J. Rekstad *et al.*, Phys. Scr., T **5**, 45 (1983).

[11] M. Guttormsen, T. Ramsøy, and J. Rekstad, Nucl. Instr. Meth. A **255**, 518 (1987).

[12] D. M. Brink, Ph.D. thesis, Oxford University, 1955.

[13] P. Axel, Phys. Rev. **126**, 671 (1962).

[14] T. von Egidy and D. Bucurescu, Phys. Rev. C **72**, 044311 (2005); see also Phys. Rev. C **73**, 049901(E) (2006).

[15] S. I. Sukhoruchkin and Z. N. Soroko, *Tables of Proton and α-Particle Resonance Parameters, Part 2: Z = 19–83* (Springer, Berlin, Heidelberg, 2005), Vol. I/19A2.

[16] A. Voinov, M. Guttormsen, E. Melby, J. Rekstad, A. Schiller, and S. Siem, Phys. Rev. C **63**, 044313 (2001).

[17] M. Guttormsen *et al.*, Phys. Rev. C **71**, 044307 (2005).

[18] J. Kopecký and M. Uhl, in *Proceedings of a Specialists' Meeting on Measurement, Calculation and Evaluation of Photon Production Data*, NEA and ENEA, edited by C. Coceva, A. Mengoni, and A. Ventura (NEA, France, 1994).

[19] S. Siem *et al.*, AIP Conf. Proc. **1090**, 66 (2009).

[20] U. Agvaanluvsan *et al.*, Phys. Rev. C **70**, 054611 (2004).

[21] M. Guttormsen, A. Bagheri, R. Chankova, J. Rekstad, S. Siem, A. Schiller, and A. Voinov, Phys. Rev. C **68**, 064306 (2003).

[22] P. Bednarczyk *et al.*, Phys. Lett. B **393**, 285 (1997).

[23] A. J. Koning, S. Hilaire, and S. Goriely, Nucl. Phys. A **810**, 13 (2008).

[24] S. Goriely, S. Hilaire, and A. J. Koning, Phys. Rev. C **78**, 064307 (2008).

[25] R. Capote *et al.*, Nucl. Data Sheets **110**, 3107 (2009).

[26] N. U. H. Syed *et al.*, Phys. Rev. C **80**, 044309 (2009).

[27] A. Voinov *et al.*, Phys. Rev. Lett. **93**, 142504 (2004).

[28] A. Voinov *et al.*, Phys. Rev. C **81**, 024319 (2010).

[29] A. C. Larsen *et al.*, Phys. Rev. C **83**, 034315 (2011).

[30] A. C. Larsen and S. Goriely, Phys. Rev. C **82**, 014318 (2010).